Construction of Strawberry-like $Ni_3S_2@Co_9S_8$ Heteronanoparticle-Embedded Biomass-Derived 3D N-doped Hierarchical Porous Carbon for Ultrahigh Energy Density Supercapacitors

Shifu Wang,[a] Zuoyi Xiao,[a]* Shangru Zhai,[a] Haisong Wang,[a] Weijie Cai,[a] Longfei Qin,[a] Jianying Huang,[a] Di Zhao,[a] Zhongcheng Li[b] and Qingda An[a]*

a. *Faculty of Light Industry and Chemical Engineering, Dalian Polytechnic University, Dalian 116034, P. R. China.*

b. *Key Laboratory of Optic-electric Sensing and Analytical Chemistry for Life Science, MOE, College of Chemistry and Molecular Engineering, Qingdao University of Science and Technology, Qingdao 266042, China*

*Corresponding authors.

E-mail: zyxiao80@163.com (Prof. Z. Xiao), anqingdachem@163.com (Prof. Q. An).

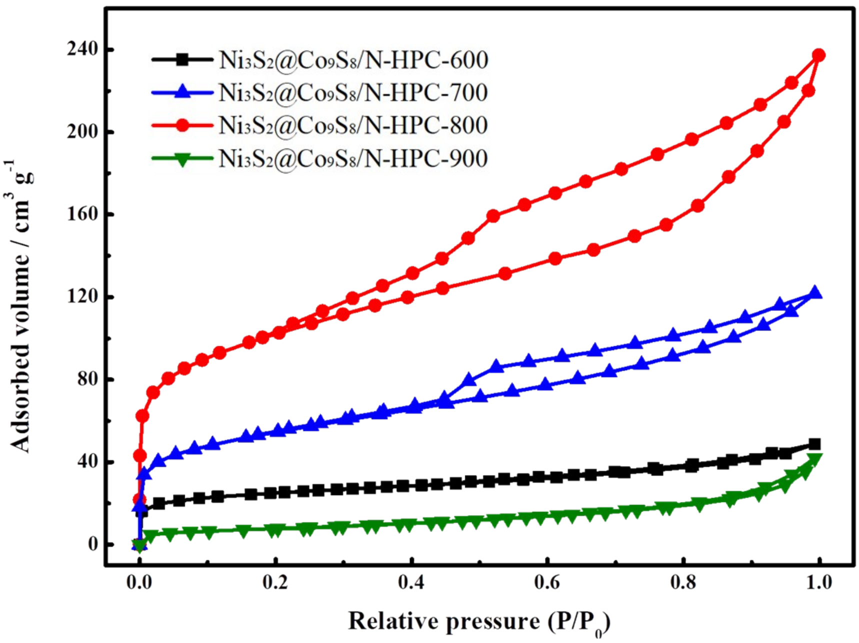

Fig. S1 Nitrogen adsorption-desorption isotherms of Ni_3S_2@Co_9S_8/N-HPC-600, Ni_3S_2@Co_9S_8/N-HPC-700, Ni_3S_2@Co_9S_8/N-HPC-800 and Ni_3S_2@Co_9S_8/N-HPC-900.

Table S1 Structural parameters of $Ni_3S_2@Co_9S_8$/N-HPC-600, $Ni_3S_2@Co_9S_8$/N-HPC-700, $Ni_3S_2@Co_9S_8$/N-HPC-800 and $Ni_3S_2@Co_9S_8$/N-HPC-900.

Sample	S_{BET} ($m^2\ g^{-1}$)	S_{mic} ($m^2\ g^{-1}$)	V_{pore} ($cm^3\ g^{-1}$)	V_{mic} ($cm^3\ g^{-1}$)	Average pore size (nm)
$Ni_3S_2@Co_9S_8$/N-HPC-600	122.8	76.7	0.075	0.017	4.58
$Ni_3S_2@Co_9S_8$/N-HPC-700	274.7	84.6	0.186	0.017	4.98
$Ni_3S_2@Co_9S_8$/N-HPC-800	360.1	73.7	0.258	0.106	5.29
$Ni_3S_2@Co_9S_8$/N-HPC-900	46.2	12.9	0.068	0.003	6.19

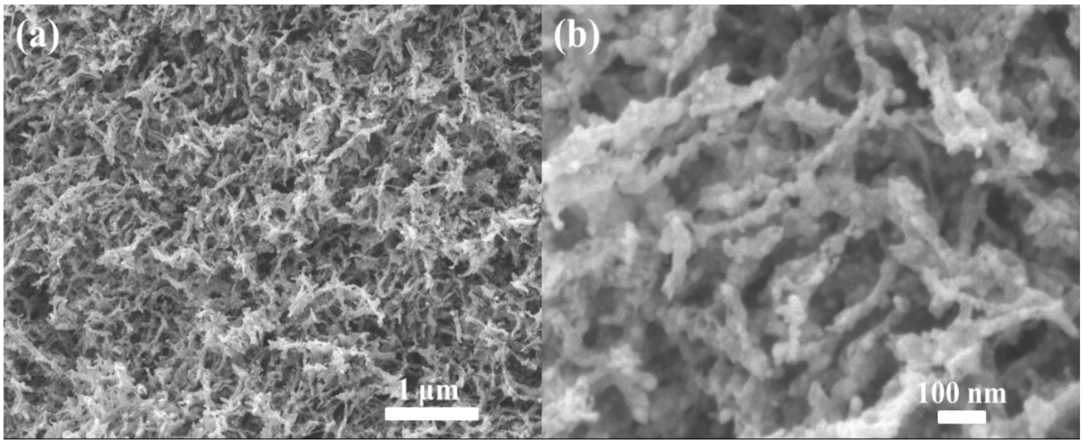

Fig. S2 (a-b) SEM images of Ni_3S_2@Co_9S_8/N-HPC-900 at different magnifications.

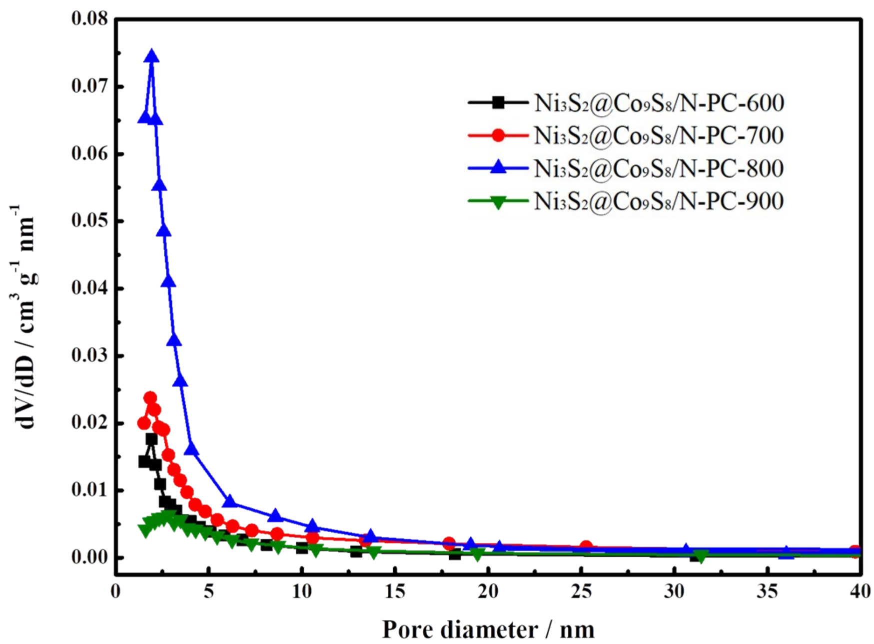

Fig. S3 Pore distribution diagrams of Ni_3S_2@Co_9S_8/N-HPC-600, Ni_3S_2@Co_9S_8/N-HPC-700, Ni_3S_2@Co_9S_8/N-HPC-800 and Ni_3S_2@Co_9S_8/N-HPC-900.

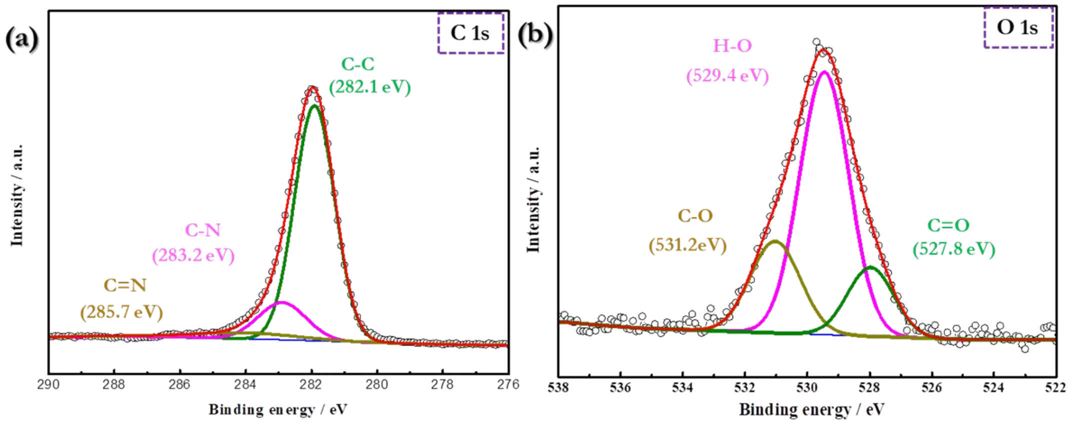

Fig. S4 High-resolution C 1s and N 1s XPS spectra of Ni_3S_2@Co_9S_8/N-HPC-800.

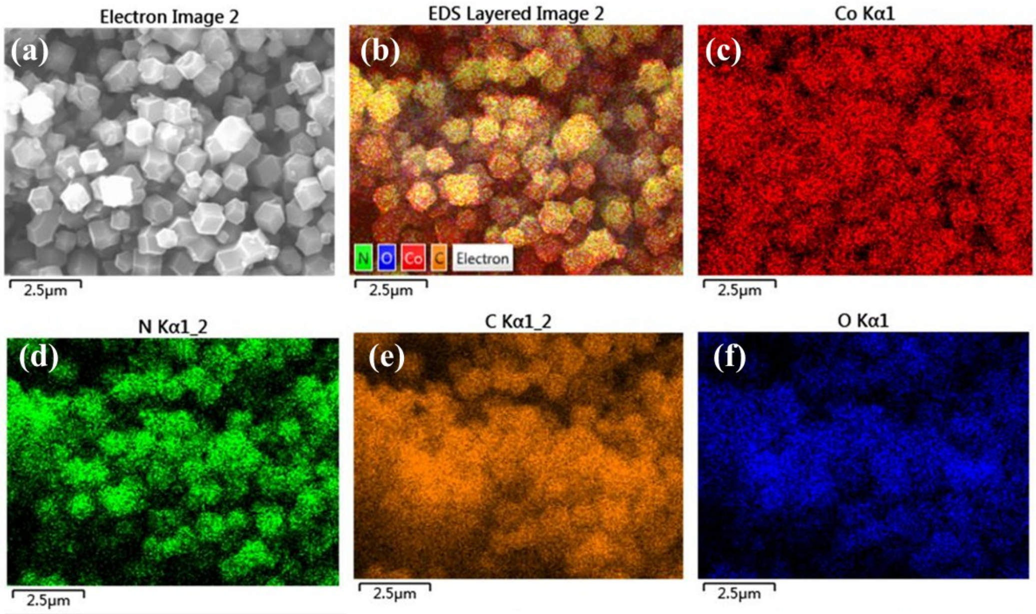

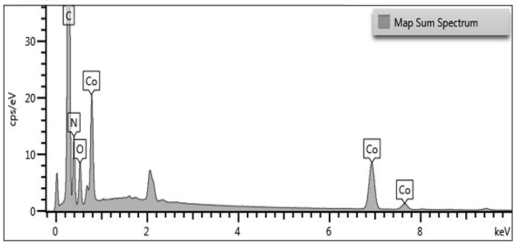

Element	Line Type	Wt%	Atomic %
C	K series	56.73	75.34
N	K series	12.17	13.86
O	K series	3.28	3.27
Co	K series	27.82	7.53
Total:		100.00	100.00

Fig. S5 (a-f) EDS mapping of the ZIF-NC-800. Map sum spectrum and the content of different elements on the surface of ZIF-NC-800.

Table S2 The content of different elements on the surface of ZIF-NC-800 and Ni_3S_2@Co_9S_8/N-HPC-800.

Element	ZIF-NC-800 (At. %)	Ni_3S_2@Co_9S_8/N-HPC-800 (At. %)
C1s	83.59	75.62
N1s	8.35	3.65
O1s	6.12	14.54
S2p	0.00	1.66
Co2p	1.38	1.57
Ni 2p	0.00	2.96

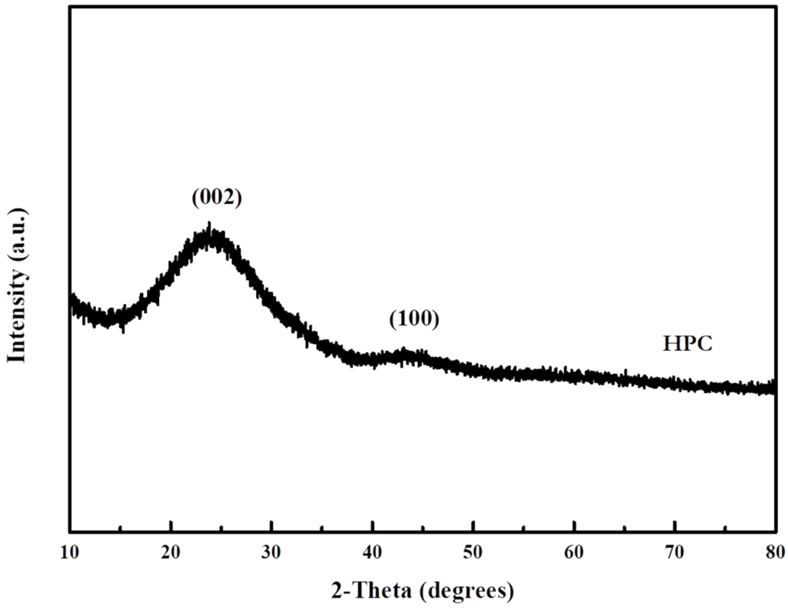

Fig. S6 XRD pattern of HPC.

Table S3 Structural parameters of HPC.

Samples	S_{BET} (m^2 g^{-1})	V_{pore} (cm^3 g^{-1})	Pore size (nm)
HPC-700	438.1	0.758	8.54

Table S4. Comparison of the specific capacitance of $Ni_3S_2@Co_9S_8$/N-HPC-800 with other reported works.

materials	capacitance ($F\ g^{-1}$)	current density ($A\ g^{-1}$)	electrolyte	reference
CoS_x/S	618	2	1 M KOH	1
CoS nanocages	1475	1	1 M KOH	2
$Ni_{3x}Co_{3-3x}S_4$	696	1	6 M KOH	3
Ni-Co-S/NF	1406.9	0.5	1 M KOH	4
Co_9S_8/NS-C	734	1	6 M KOH	5
NiCo-MOF	1202.1	1	2 M KOH	6
Ni_3S_2	1370.4	2	6 M KOH	7
Ni@rGO-Ni_3S_2	987.8	1.5	6 M KOH	8
NF@rGO/Ni_3S_2	816.8	0.98	6 M KOH	9
$Ni_3S_2@Co_9S_8$/N-HPC-800	1970.5	0.5	6 M KOH	This work

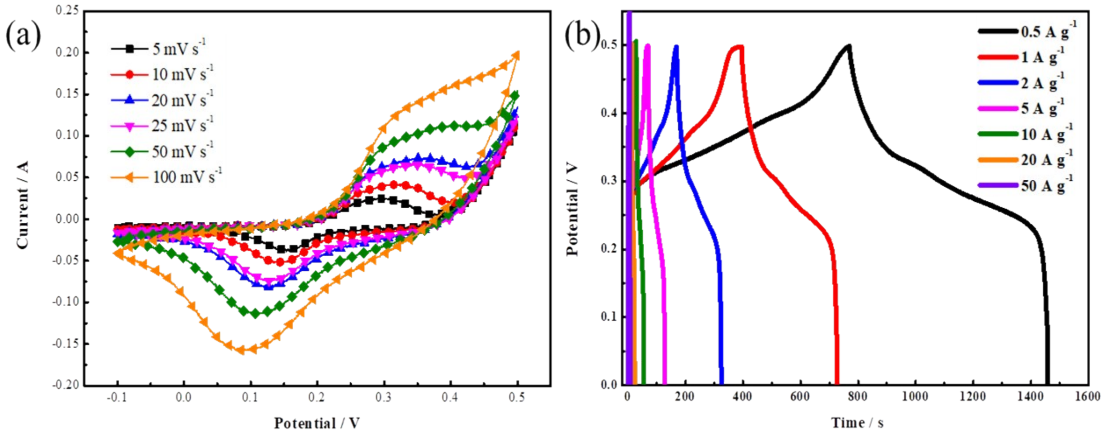

Fig. S7 (a) CV curves at different scan rates from 5 to 100 mV s^{-1}, (b) GCD curves at various current densities for Ni_3S_2@Co_9S_8/N-HPC-600.

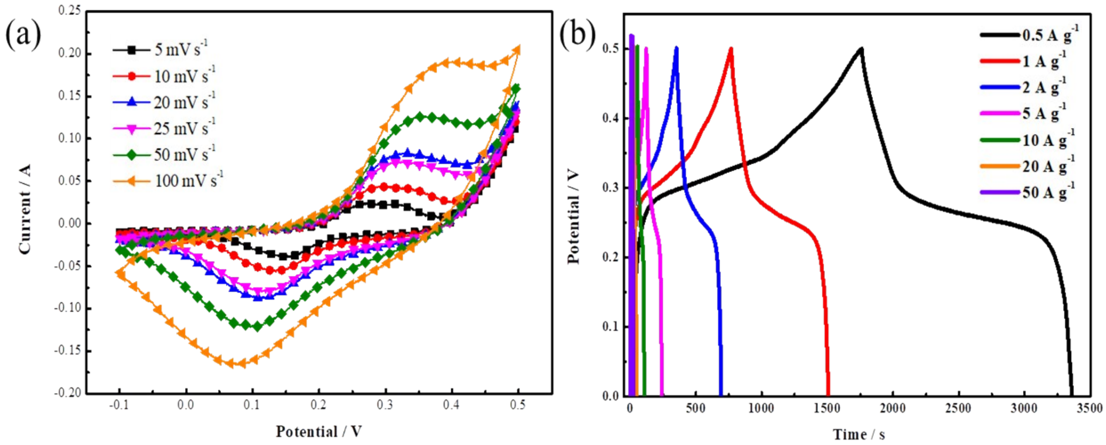

Fig. S8 (a) CV curves at different scan rates from 5 to 100 mV s^{-1}, (b) GCD curves at various current densities for Ni_3S_2@Co_9S_8/N-HPC-700.

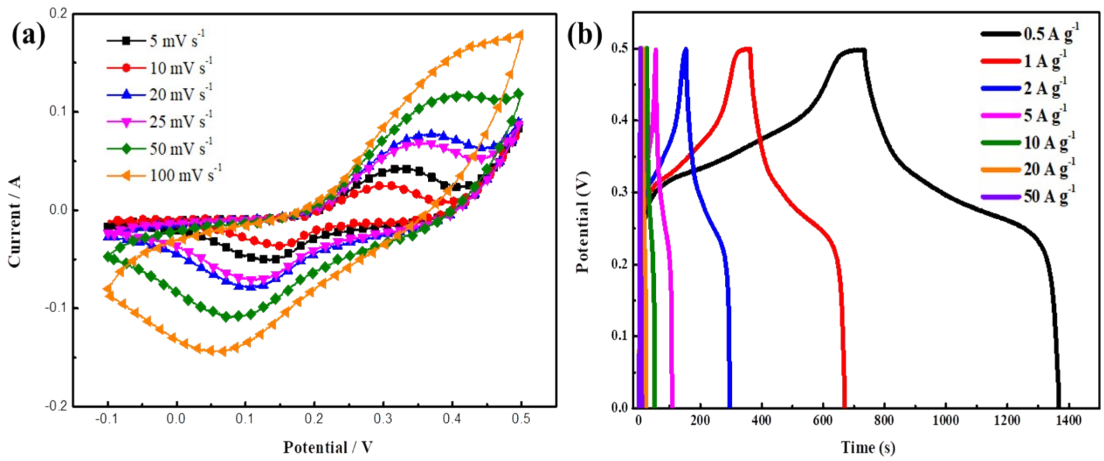

Fig. S9 (a) CV curves at different scan rates from 5 to 100 mV s^{-1}, (b) GCD curves at various current densities for Ni_3S_2@Co_9S_8/N-HPC-900.

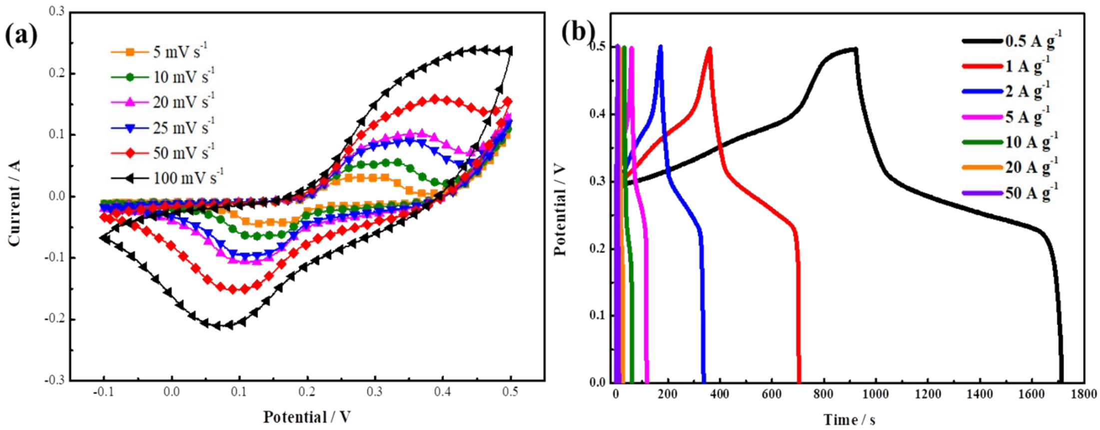

Fig. S10 (a) CV curves at different scan rates from 5 to 100 mV s^{-1}, (b) GCD curves at various current densities for Co_9S_8/N-HPC-800.

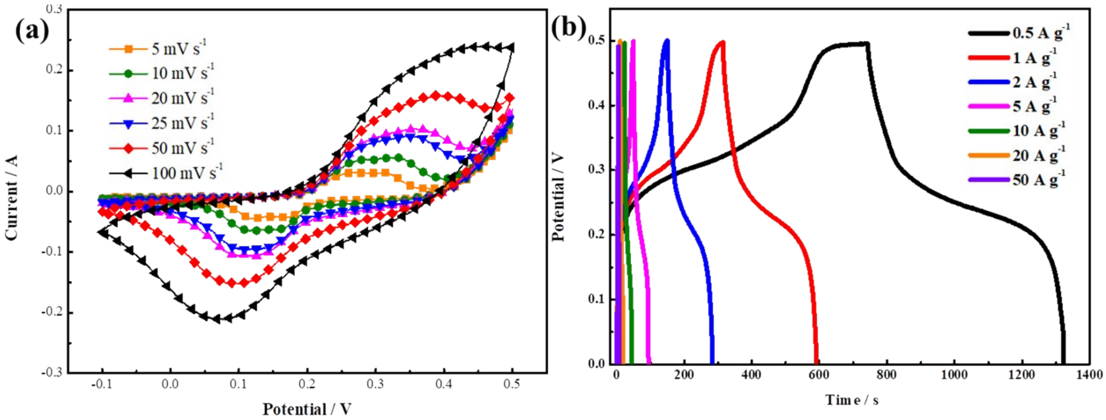

Fig. S11 (a) CV curves at different scan rates from 5 to 100 mV s^{-1}, (b) GCD curves at various current densities for Ni_2S_3/N-HPC-800.

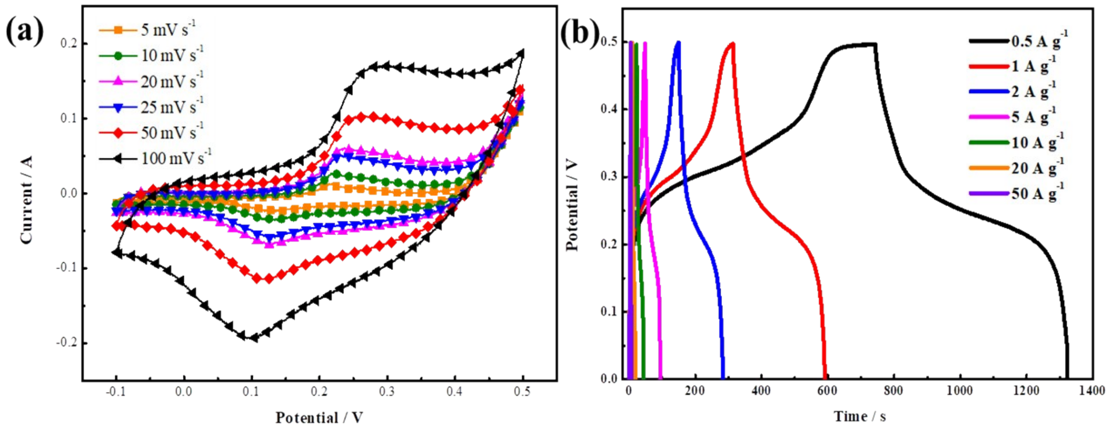

Fig. S12 (a) CV curves at different scan rates from 5 to 100 mV s^{-1}, (b) GCD curves at various current densities for ZIF-NC-800.

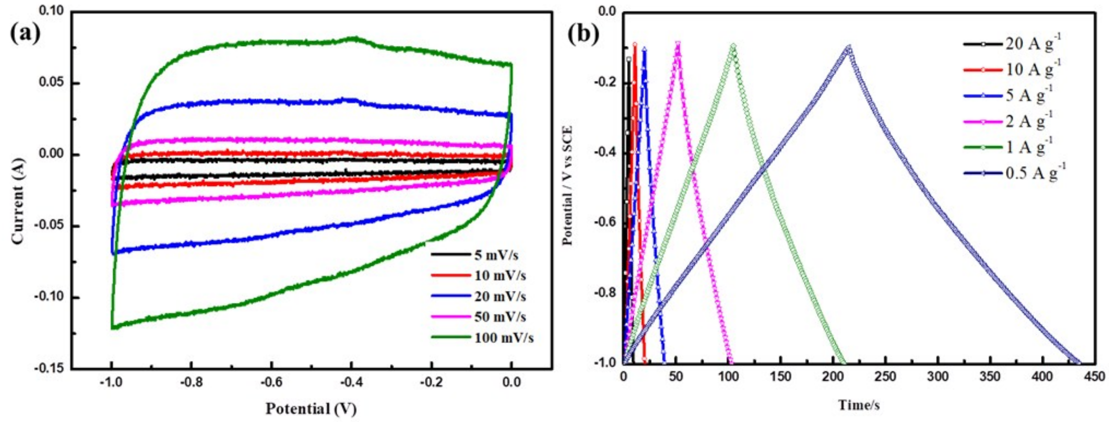

Fig. S13 (a) CV curves at different scan rates from 5 to 100 mV s^{-1}, (b) GCD curves at various current densities for HPC.

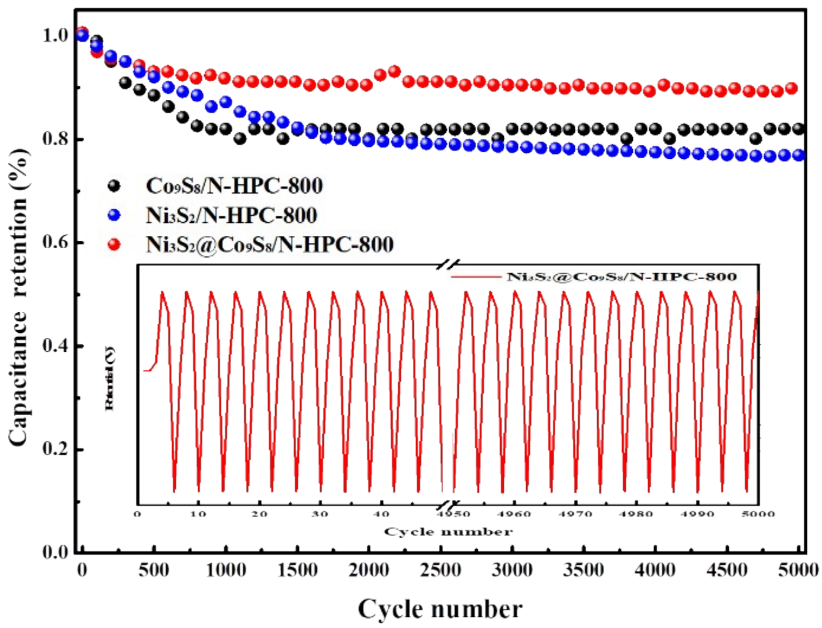

Fig. S14. Comparison of the cycling stability of Ni_3S_2/N-HPC-800, Co_9S_8/N-HPC-800 and Ni_3S_2@Co_9S_8/N-HPC-800.

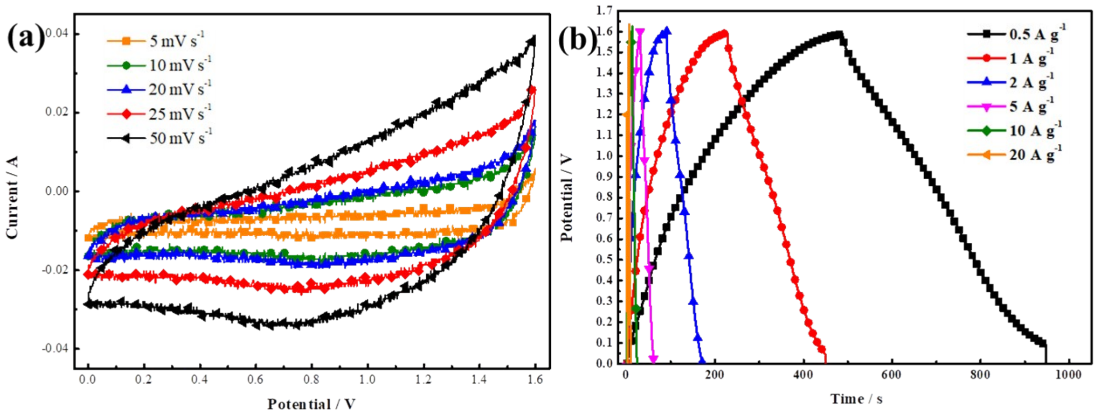

Fig. S15 (a) CV curves at different scan rates and (b) GCD curves at different current densities of the Co_9S_8/N-HPC-800//HPC asymmetrical supercapacitor.

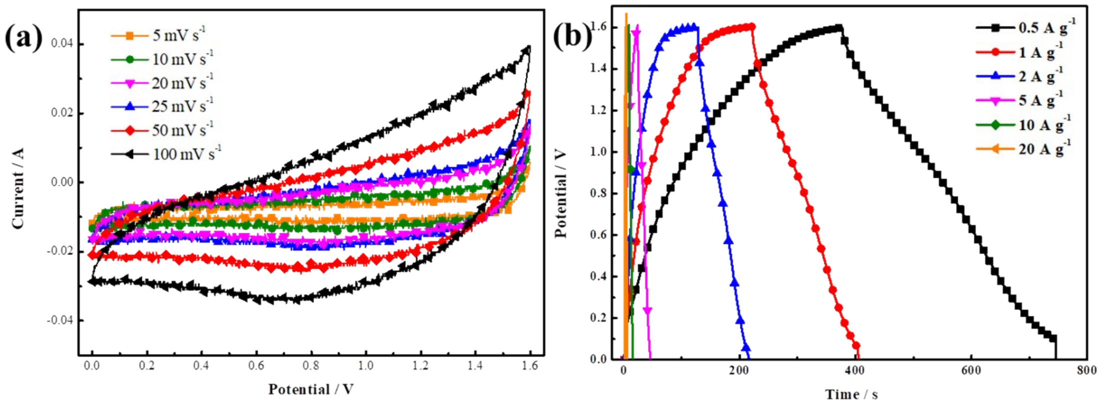

Fig. S16 (a) CV curves at different scan rates and (b) GCD curves at different current densities of the Ni_3S_2/N-HPC-800//HPC asymmetrical supercapacitor.

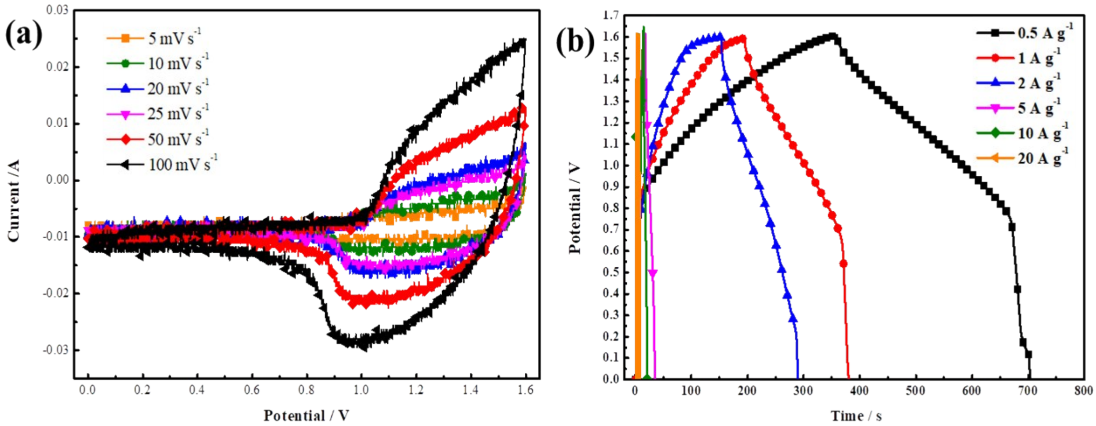

Fig. S17 (a) CV curves at different scan rates and (b) GCD curves at different current densities of the ZIF-NC-800//HPC asymmetrical supercapacitor.